Photonics and Nanostructures - Fundamentals and Applications 48 (2022) 100985

Contents lists available at ScienceDirect

Photonics and Nanostructures - Fundamentals and Applications

journal homepage: www.elsevier.com/locate/photonics

Eliminating excess phase accumulation in a continuous perturbed heterogeneous planar photonic crystal

Shahram Moradi [a,b], Mahdi Zavvari [c,*], Yashar Zehforoosh [c], Armin Arashmehr [c], Jens Bornemann [a]

[a] Department of Electrical and Computer Engineering, University of Victoria, Victoria, Canada
[b] Micro and Nano Technology Department, Middle East Technical University, Ankara, Turkey
[c] Microwave and Antenna Research Center, Urmia Branch, Islamic Azad University, Urmia, Iran

ARTICLE INFO

Keywords:
Excess phase accumulation
Continuous perturbation
Planar photonic crystal
Negative group delay

ABSTRACT

We propose an asymmetric distribution of a hexagonal lattice for achieving near-zero group velocity with negative group delay. This study reports the effect of the continuous geometric perturbation on the photonic band diagram and consequently its impact on phase velocity, group velocity, and effective refractive index. We provide a promising method for modifying the photonic band diagram to obtain an exotic dispersion diagram. With this broadband spanning from the E band to the L band, the light pulse envelope travels with almost zero velocity and is promising for application in a wide variety of light-based devices.

1. Introduction

Planar photonic crystals [1] control localized slow light by slowing down the group velocity and are of interest in many light-based devices, such as photonic integrated circuits [2], waveguides [3,4], wide-band reflectors [5], filters [6], lasers [7], and multimode guided wave lenses [8,9]. Group velocity (v_g) is the phase response [10,11] of a medium that is computed through the derivative of the phase velocity v_p with respect to a certain range of frequencies.

A light pulse containing a series of sine waves that each experiences different phase responses can be steered via dexterous engineering matter. The dispersion diagram as a result of this diversity in phase response in an artificial material provides useful information that explains how a light pulse envelope interacts with matter during propagation in a transmission path. Three types of dispersion occur in various types of optical components, including artificial and/or normal media: no dispersion (v_g=v_p), normal dispersion (v_g<v_p), and anomalous dispersion ($v_g > v_p$).

In terms of applications, shortening or reducing transmission delays can play a critical role in ultrahigh optical switching elements [12] and today's complex modulation techniques in modern RF wireless communicating platforms [12]. In addition, all-optical regeneration of a signal [13] is desired to avoid polarization mode dispersion [14,15], eliminate influences of noise, and reduce limitations associated with wavelength-division multiplexed transmission [16].

Transmitting a light pulse through a chromatic dispersive material with high accuracy, low loss, and no distortion in fiber optics and/or any on-chip elements is a hard task. However, an advance in phase compensates for positive group delay of the transmission line and also assists in increasing the efficiency of amplifiers [17,18]. Negative group delay [19] as a unique phenomenon gives rise to an advance in phase, which does not occur in most transmission lines of electromagnetic waves. Considering a traversing electromagnetic wave through a dispersive material, an envelope of magnitude experiences an advanced shift rather than delay via negative group delay.

This promising effect has been studied in both electronic circuitry [20,21] and high-frequency structures [22,23]. For $e^{ik(\omega)z}$ as a transfer function of a normalized plane wave propagating along the z-axis, its complex wave number is $k(\omega) = \alpha(\omega) + i\beta(\omega)$. The corresponding phase and group delays at any particular point on the z-axis are

$$T_p = \frac{z}{v_p} = \frac{\alpha(\omega)}{\omega} z, \quad T_g = \frac{z}{v_g} = \frac{\mathrm{d}}{\mathrm{d}\omega}(\alpha(\omega))z,$$

where v_p and v_g are the phase velocity and the group velocity, respectively. Furthermore, according to Sommerfeld, the front end of the wave packet with velocity v_f has the speed of light (c) in a vacuum since

* Corresponding author.
E-mail address: m.zavvari@iaurmia.ac.ir (M. Zavvari).

https://doi.org/10.1016/j.photonics.2021.100985
Received 21 January 2021; Received in revised form 30 September 2021; Accepted 2 December 2021
Available online 10 December 2021

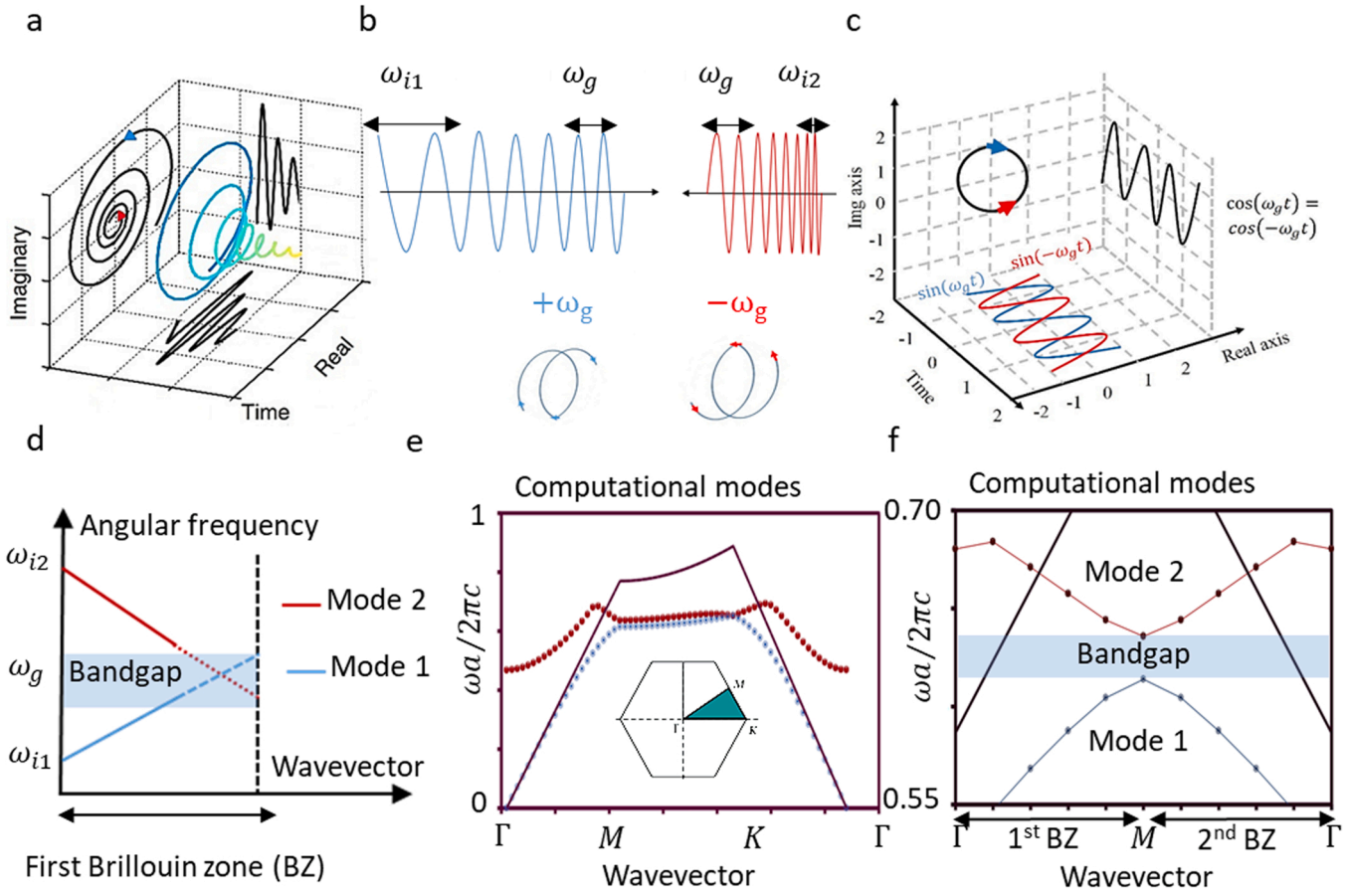

Fig. 1. Interaction of waves (wave packet) and types of group delays. (a) Time variation transition of a wave packet through real space form either ascendant to descendant group velocities or vice versa. (b) Two-dimensional wave transition from the initial frequency ω_i to the frequency with the dominant group velocity ω_g forms either $+\omega_g$or$-\omega_g$, which are different in the directions of motion. (c) Trajectories of two possible envelopes that differ in sine components and are the same in the cosine component. (d) Cancelation of two modes due to the opposite gradient of envelope transitions. (e) The dimensionless quantity $\omega a/2\pi c$ with lattice constant $a = 0.5$ μm versus the wavevector in a hexagonal lattice printed in a silicon slab with a thickness of 0.32 μm on top of a 1 μm silicon dioxide substrate. (f) Zoomed-in band diagram in the Γ-*M*-Γ direction showing the symmetries in the optical path with the creation of a photonic bandgap. BZ, Brillion zone.

$$T_f = \frac{z}{v_f} = \lim_{\omega\to\infty}\frac{\alpha(\omega)}{\omega}z.$$

Under such conditions, even if the rest of the envelope propagates with a superluminal velocity (negative group delay), the continuation of the advanced phase of the whole wave packet would give rise to no distortion of the traversing wave packet.

Here we study the effect of varying the density of the dielectric distribution on controlling the group index via periodic geometric transition. The suggested optical component provides a unique time-evolving wave packet from a given initial state that accumulates an advanced phase for a broadband range of wavelengths near the band edge.

This class of media, modulated photonic crystals [24], with an asymmetric nature of periodic structures exploits the unbalanced density of states not only in the first Brillouin zone but also through the entire lattice due to continuously broken symmetries. In summary, a smooth disordered hexagonal-like cluster in a two-dimensional lattice is distributed through the entire suggested component, in which the volume of air (cylindrical holes) changes only along Γ-*M*. A left-handed material with a negative gradient of the wavevector $(k'(\omega) < 0)$ forms in a periodic lattice to create negative group delay, which we discuss in this study.

2. Left-handed versus right-handed materials

Light as a wave oscillates due to the fluctuation of two components ($\vec{E}$ and $\vec{H}$) that ideally cross each other at two trajectory planes that are perpendicular to each other. From a complete wave point of view in an inhomogeneous medium with no spatial filtering, the creation of a partially polarized light pulse can be affected by either horizontal or vertical components in the case of an asymmetric distribution of either of the fields through the medium. Therefore, such propagating wave packets experience a modification in both wavelength and magnitude (Fig. 1a).

As is clear from Fig. 1, one of the arrows (red or blue) may occur in such a transition. Thus, evolving ($\vec{E}$and$\vec{H}$) fields are possible by our considering conservation of energy. In Fig. 1b, variation of only the wavelength in an inhomogeneous medium such as a photonic crystal creates two types of evolution from the initial states (ω_i), which results in a particular angular frequency of the whole envelope (ω_g), which determines the group velocity of the wave packet. In a special case, the coupled-mode theory on a subwavelength scale is based on the perturbation of the refractive index through the lattice, which explains the possibility of producing a complete backward wave scattering due to optically linear parametric interaction (Fig. 1c).

This gives rise to the coalescence of two eigenstates (Fig. 1d) near the band edge, which can result in diverse group delays. In photonics science, for an elaborate understanding of any type of dispersion in any region (linear or nonlinear) for given heterogeneous interfaces in (meta)

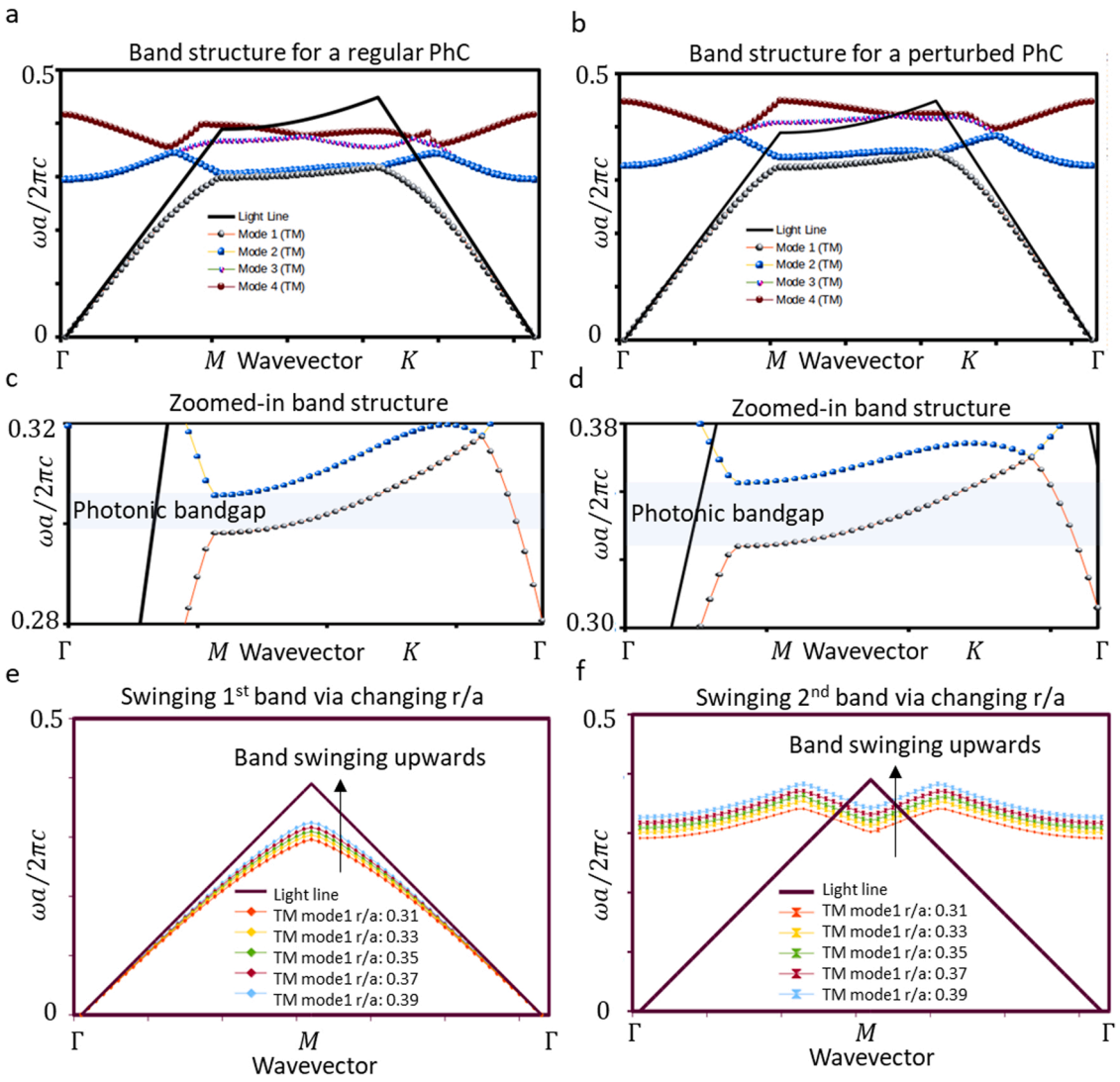

Fig. 2. Swinging band diagram for a hexagonal lattice for the suggested lattices with (a) the radii equal to 0.31 and having a photonic bandgap (PBG) around 0.3 in the Γ-*M* direction and (b) the radii equal to 0.39 and having a PBG around 0.33 in the Γ-*M* direction. (c) and (d) The zoomed-in PBG part of the photonic bandgaps in (a) and (b), respectively. (e) Swinging of the first band to the higher angular frequencies with increase of the radii. (f) Swinging of the second band to higher angular frequencies with increase of the radii. PhC, photonic crystal; TM, transverse magnetic.

material, there should be a map to steer light in a dexterous manner. For instance, computation of the band diagram is a necessary step to have a seminal record of electromagnetic waves interacting with any type of matter, including homogeneous or inhomogeneous matter.

Thus, instead of the use of time-independent Schrödinger equation [25], use of the master equation, which is the so-called eigenvalue equation [26], produces eigenvalues of all possible states. By consideration of the linearity of the Maxwell equation for both fields in time, $E(r,t) = E(r)e^{i\omega t}$ and $H(r,t) = H(r)e^{i\omega t}$, the solution via Fourier theory will not construct the possible solutions for its given components. Instead, the combination of all propagating modes (Bloch envelope) as a solution for both fields can be obtained by solving the given master equation with reference to each of the computed ω [27]. To have a clear image of the propagation modes as a solution for the Maxwell equations, one needs to eliminate the electric field E and apply the Bloch envelope for broken symmetries in the two fields and a transverse guiding mode for only the magnetic field H [27]:

$$\Theta \quad H(r) = \left(\frac{\omega}{c}\right)^2 H(r),$$

where $\Theta H(r) \equiv \nabla \times \left(\frac{1}{\varepsilon(r)} \nabla \times H(r)\right)$ exhibits a functional form of the dielectric to determine the magnetic field. If we consider Hamiltonian system for the suggested system, since the Hermitian operator (Θ) derives all eigenstates for the magnetic fields, the determination of eigenstates for the electric field would be the next step. Therefore, applying a translation of any symmetry, such as in a photonic crystal, gives rise to the dispersion relation in which the splitting bands are expected.

Implementing Bloch's theorem via the computational tool MIT Photonic Bands (MPB) [28], we conducted a simulation with a high-resolution finite-element method in which the grid elements for a three-dimensional structure, a hexagonal lattice, were applied. The computed photonic band structure for such a lattice (cylindrical air) printed in a silicon film with a thickness of 0.32 μm on top of 1 μm silicon dioxide as a substrate is depicted in Fig. 1e.

The suggested photonic crystal possesses propagating modes for both transverse electric (TE)-like polarization and transverse magnetic (TM)-like polarization. However, the group index of the TM-like mode is higher than that of TE-like mode, giving rise to a slow light mode [29]. In addition, the evolutions of TE-like and TM-like modes are dissimilar because of the different wave equations. Furthermore, the bandgap closure and band flips via any perturbation parameters affect only

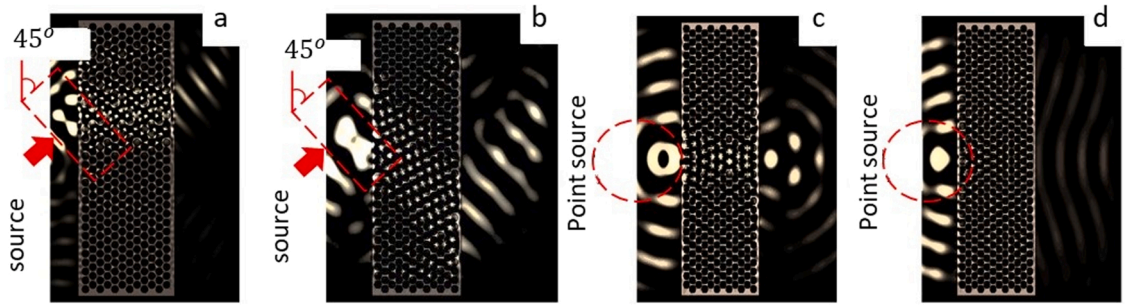

Fig. 3. Light flow through the photonic crystal ($a = 0.5$ μm, silicon thickness 0.32 μm, silicon dioxide thickness 1 μm) illustrating first-order dispersion in (a) right-handed material, (b) left-handed material interacting with a 45° tilted plane wave source, (c) left-handed material, and (d) right-handed material interacting with a point source.

TM-like bands rather than TE-like modes. This is due to the symmetry properties of the band edge in TM-like modes [30].

In Fig. 2, we show results of calculations for only the TM mode, which corresponds to the eigenmodes of the *z*-component of an applied electric field (E_z) in the proposed hexagonal lattice, summarized in three directions (Γ, M, and K) due to two-dimensional symmetries in the first Brillouin zone. Furthermore, bands computed with the finite-element method show power disintegration along the photonic bandgap in the Γ-M direction. However, the light flow is deviated to the other symmetry direction due to joining of computed bands at the K points.

Thus, we expect a symmetric band diagram in the second Brillouin zone due to the symmetric nature of the lattice in one of the directions (Fig. 1f). This diagram provides seminal information for steering light in an engineered material. For instance, for such a photonic band structure, both the left-handed material zone and the right-handed material zone of a designed photonic crystal can be recognized because of different gradients of wavevectors introduced around the photonic bandgap. In addition, this zone is subjected to geometric order and swings via any variation of the design parameters. For example, we can achieve a swinging stopband along with the communication range of frequencies by means of either perturbation of the lattice or changing one design parameter, such as the lattice constant or a radius.

In Fig. 2, the swinging stopband is depicted for both bands separately. Since the gradient of the wavevector $k(\omega)$ takes both negative and positive values in each portion of the photonic bandgap (positive values for the first band and negative values for the second band) with respect to the direction of propagation in the reciprocal lattice (e.g., in the Γ-M direction), the type of dispersion follows these different values as well.

However, we can examine this phenomenon only from the transmission spectrum, but the band structure provides more specific information about the effect of changing any parameter on any of the specific modes through the computed dispersion diagram. This also helps us to calculate the gradient of the wavevector (e.g., first and second order) with respect to the given frequency ω in both reciprocal space and Cartesian space. Furthermore, we want to show the effect of different values (either negative or positive) of the gradient of the wavevector in a photonic crystal.

In Fig. 3, we provide a slice of an unsteady simulation performed with the finite-difference time-domain method for the two-dimensional hexagonal lattice to specify differences in any type of chromatic dispersion. In other words, left-handed materials and right-handed materials are the result of chromatic dispersion, and both influence the angle of radiation due to the order of the phase velocity for an incident wave propagating through the lattice. According to Snell's law, the incident wave refracted from a positive index material (PIM) to a negative index material (NIM) follows the equation $n_{\mathrm{PIM}}\sin\theta_{\mathrm{PIM}} = n_{\mathrm{NIM}}\sin\theta_{\mathrm{NIM}}$ and the backward bending of the ray represents the negative angle of refraction in the photonic crystal, which is depicted in Fig. 3b.

Thus, satisfying Snell's law with a negative angle of refraction is possible only by multiplication with negative values of the refractive indices. As a result, the subscripts NIM and PIM are assigned to parameters in the equation for accurate analysis of chromatic dispersion in left-handed materials. In Fig. 3b, the nature of first-order dispersion varies for the same light pulse profile but different radii since chromatic dispersion depends on the gradient of the wavevector as it follows the band diagram. So, any perturbation in geometry gives rise to a swinging photonic band diagram, and reconstruction of different values of the group velocity $(k'(\omega) \equiv \partial k/\partial\omega = 1/v_g)$ is a possible method.

Consequently, we conclude that changing the optical parameters in the geometry of lattices such as radii or the lattice constant gives rise to different types of first-order dispersion. All in all, for a particular frequency range, the gradient of the wavevector $(\frac{\partial k}{\partial\omega}, \frac{\partial^2 k}{\partial\omega^2})$ can be either negative or positive, which influences the nature of the dispersion. However, to create a broadband negative refractive index to keep the entire envelope distortionless, one needs a dexterous approach to exploit the geometric effect on the photonic band diagram, which we discuss in the following section.

3. Modeling the structure via an asymmetric lattice

Per our previous discussion, use of MIT Photonic Bands as an eigenmode solver via the plane wave expansion method to obtain the accurate photonic band structure gives us a connection between given electromagnetic radiation and optical medium properties. It is worth mentioning the advantages of choosing a hexagonal lattice since it is capable of realizing a bandgap in both TM and TE modes simultaneously. In other words, proficiency of having two-dimensional symmetry in such a lattice, dielectric globs, and connective veins establish a photonic bandgap to control light efficiently.

To have a deep understanding of the origin of a possible bandgap in the suggested lattice, one needs to be aware of some fundamental notions. First of all, distributed electric fields in a lattice with two components (air and a dielectric) results in the lowest-order mode (first band) preferring to reside in higher-index regions, so it is called a *dielectric band*. Unlike the dielectric band (first band), the second-order band prefers the realization of electric field power in air (the air band). Once these two modes becomes orthogonal to each other, the creation of a gap is possible due to the interference of two waves with the same periodicity for the same frequencies (see the discussion in the caption for Fig. 1).

Thus, some band frequencies cannot propagate in that particular direction. What if we break the periodicity by changing the distribution of the dielectric? For example, reducing or increasing the diameter of the cylindrical holes (air) in a two-dimensional lattice will break the periodic dielectric continuously. According to our former results, the band structure fluctuates with respect to such variation and gives rise to swinging in the energy level with respect to the degrees of variation. We studied the effect of such variation and propose an approach to explain our novel modeling structure. The more symmetry is the more similar Bragg grating appears in the computed directions.

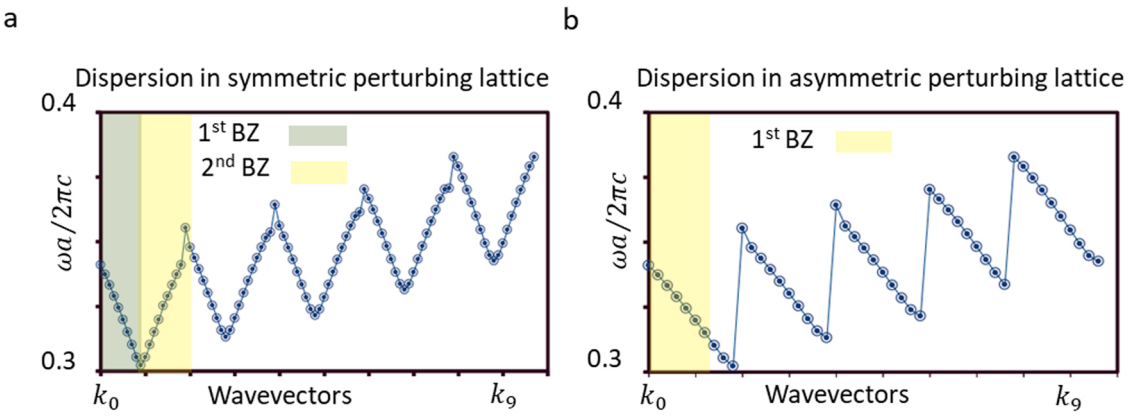

Fig. 4. Dispersion in (a) a symmetric and (b) an asymmetric perturbed hexagonal lattice. BZ, Brillion zone.

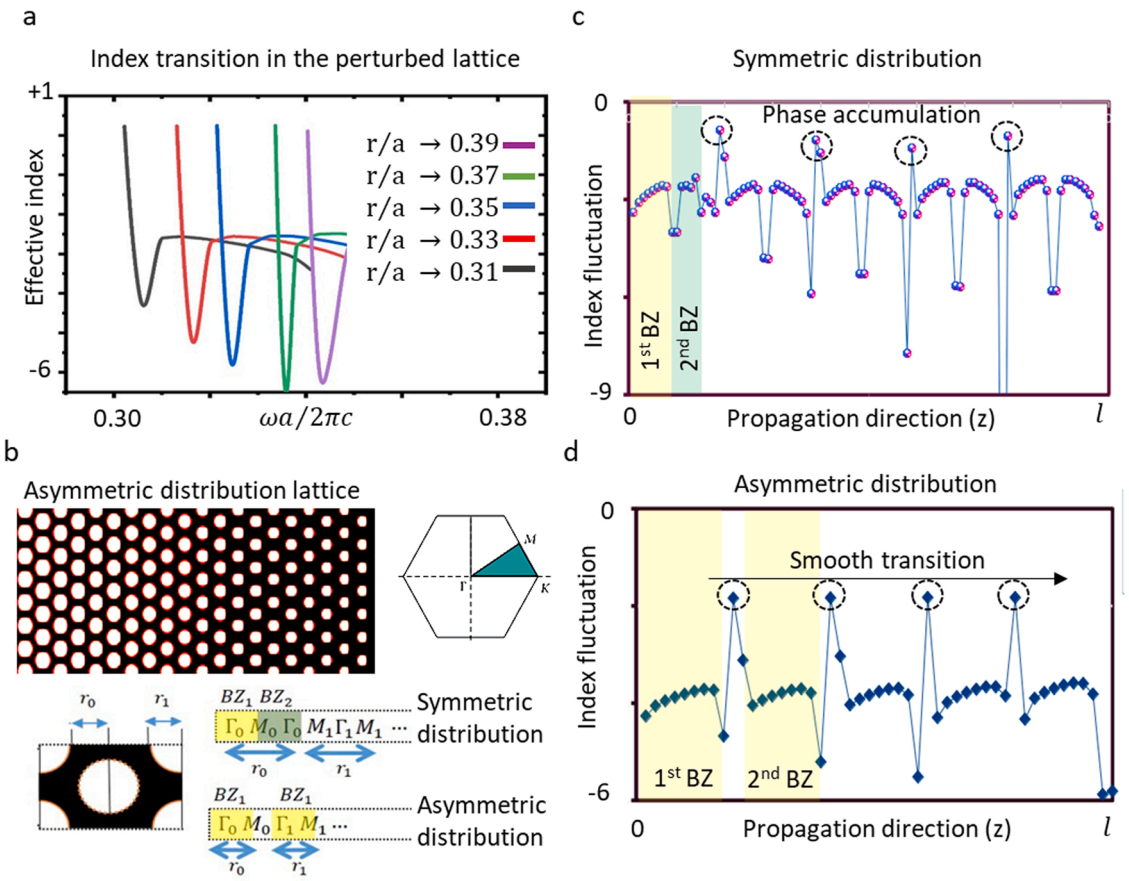

Fig. 5. (a) Effective index variation by the changing radii in a hexagonal lattice. (b) An asymmetric hexagonal lattice and a unit cell possessing perturbed radii that create a different path in the reciprocal space. (c) Refractive index fluctuation through the entire lattice for a symmetric hexagonal lattice showing excess phase accumulation in the propagation direction. (d) Refractive index fluctuation through the entire lattice for a asymmetric hexagonal lattice showing excess phase accumulation in the propagation direction. BZ, Brillion zone.

Otherwise, the cancelation of two bands will be replaced with the accumulation of phase. In other words, applying a linear variation of the radii in each column (unit cell) in a hexagonal lattice gives rise to dynamic variation of the wavevector as it is propagating through the lattice. Let us assume propagation incident in the Γ-*M* direction and that the radius of unit cells in the *z*-direction varies ($\Delta r = D_2 - D_1$) smoothly to avoid any Fresnel reflection based on no optical impedance mismatch. Because of the dependency of the wavevector on changing radii, the gradient of the wavevector with respect to the frequency ($\partial k(z)/\partial\omega$) will be either descendant (negative) or ascendant (positive). Thus, the type of chromatic dispersion can vary, as shown in Fig. 4.

We applied a Gaussian pulse to compute the transmission spectrum of both structures including an ascendant and a descendant dielectric volume distributed in the lattice. We used the finite-difference time-domain method in MIT Electromagnetic Equation Propagation (Meep) [31] to illustrate different optical properties in the transmission spectrum for a particular frequency range in both disordered lattices. The simulation was done in our suggested three-dimensional structure with a two-dimensional photonic crystal array of cylindrical holes (air) printed in silicon film with a thickness of 0.32 μm on 1 μm silicon dioxide as a

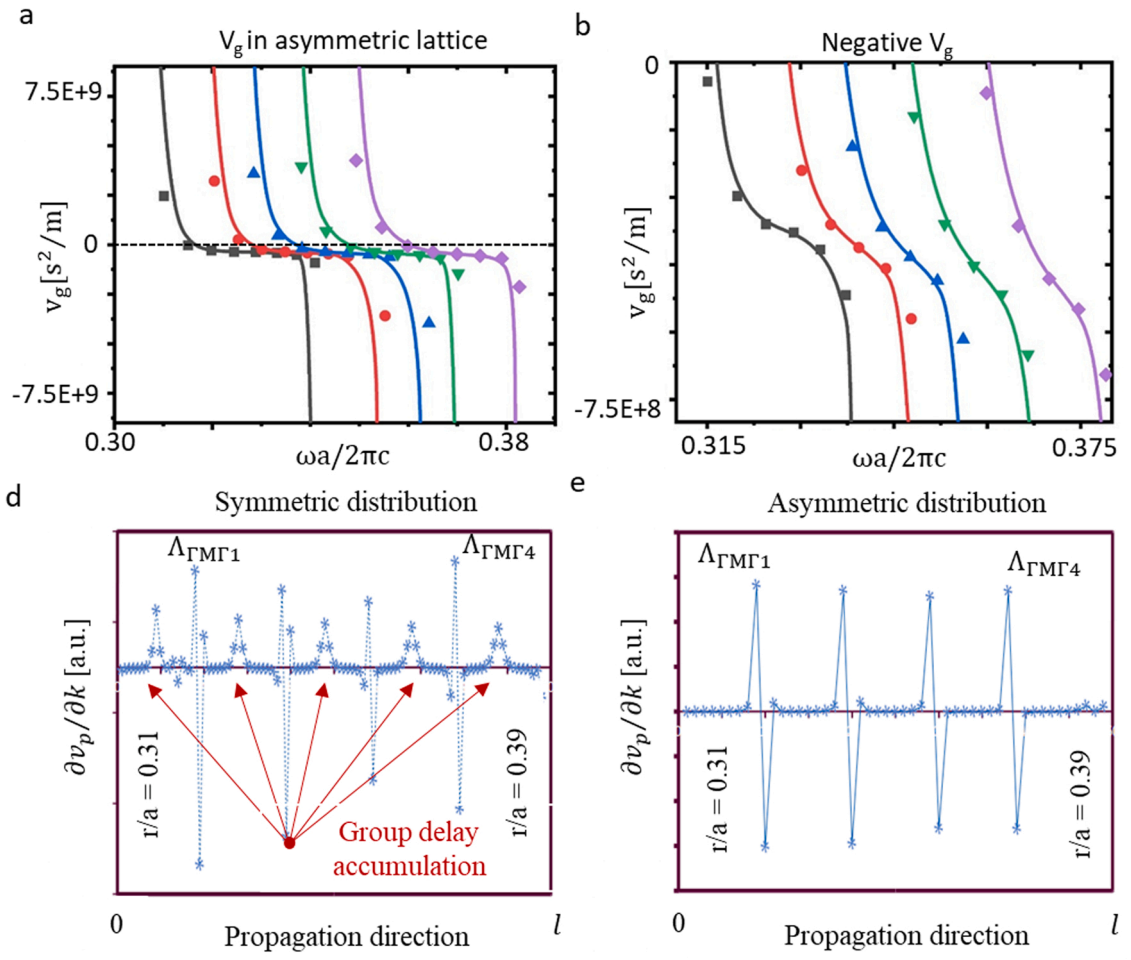

Fig. 6. (a) Group velocity with radii varying from 0.31 (black) to 0.39 (pink) and (b) the zoomed-in region with negative group velocity. (c) The symmetric distribution accumulates group delay in each transition from the first Brillouin zone to the second one and weak compensation for the transition of perturbing radii. (d) Asymmetric distribution with smooth group delay and compensating group delay in each transition of perturbing radii.

substrate.

Our suggested metamaterial composed of multiple clustering hole meshes generates an exotic band diagram because of broken symmetries. This platform can be used to control the density of states near the band via continuous perturbation of parameters (radii) and to widen the negative band in the communication wavelength range.

In Fig. 5a, the refractive index with negative values fluctuates, while the radii change from 0.31 to 0.39 in the lattice shown (Fig. 5b). As is clear from Fig. 5a, the negative effective index covers the bandwidth in the telecom range consisting of the extended band E, the short band S, the conventional band C, and the long band L. However, this broadband negative index region has functionality depending on the orientation (Γ-*M*). Thus, this broadband functionality is based on connectivity rather than a consequence of resonating electromagnetic waves in subwavelength structures. In Fig. 5c, the proposed lattice with continuous perturbation of radii shows two types of distributions: one with a symmetric hexagonal lattice that consists of two Brillouin zones and the other a cluster, for which before entering the symmetric second, Brillouin zone, light traverses to the perturbed stack. To understand the difference in the types of distributing clusters, one can determine their effective refractive index fluctuation through the Γ-*M* light path shown in Fig. 5b–d. The perturbing effect in these two sections merely provides radii for 0.31–0.39 in four steps, which is not what the real structure under study refers to. In other words, the proposed structure experiences perturbed radii with very smooth transitions of radii to have lengthy devices for realistic applications.

For broadband propagation, light pulses are distorted because of different phase velocities at each frequency. Thus, the complexity of signals at the end of the light path is inevitable because of the generation of multiple intrinsic modes that each exhibit nonlinear group delay. Dispersion is a characteristic originating from the environment (media) and depends on the properties of the source as well. That is why characterizing the group delays extracted from each mode is considered indispensable, and is used as a parametric inversion to retrieve the signal containing the information. Here we show the difference between two suggested structures with specific group delays.

In Fig. 6, the type of distributing clusters in a specific lattice, continuously perturbed radii, influences the group delay in any transition through the light path. According to the gradient of phase velocities of the symmetric distribution and the asymmetric distribution, the one that does not enter the second Brillouin zone experiencing the perturbation effect has a smooth group delay rather than the cluster with the symmetric distribution. In our suggested structure, the continuously perturbed lattice, which is a proper platform for broadening the band with almost zero group delay, eliminating frequent positive values of the group delay in each transition to the second Brillouin zone, plays a destructive role.

Furthermore, mismatching of the phase of two clusters with different effective refractive indices causes asymmetric values of the group delays in each interval. Therefore, the nonlinear accumulation of group delays at the end of the light path gives rise to a light pulse distorted in a complex manner. Unlike the symmetric distribution of the cluster in

photonic crystals, broken symmetries produce a proper platform that not only eliminates the accumulation of group delays in the middle of the two Brillouin zones but also provide symmetric values of the group delays in each perturbed transition, which compensate each other.

4. Conclusion

We have presented a new method of tailoring photonic crystals to form a dynamic wavevector gradient through a continuously perturbed lattice. The exotic photonic band diagram gives rise to the broadening of the band in the negative refractive index region. This unique band diagram is due to the connectivity of stacks rather than resonance in the subwavelength structure. This approach, smooth variation of the dielectric distribution, spreads the photonic band edge toward higher or lower frequencies contingent on the type of perturbation, either low to high density or high to low density. This produces broadband near-zero group delay with $k^{'}(\omega, \overrightarrow{r}) < 0$.

In addition, we compared the two types of perturbed radii through the proposed lattice. We realized both symmetric and asymmetric hexagonal clusters via modifying the unbalanced distribution of the dielectric through the entire component. The asymmetric lattice is suggested for eliminating excess phase accumulation in the light path. The suggested optical component and the reported approach provide a promising technique to obtain a unique platform for producing near-zero group delay by covering a broadband range of frequencies adjacent to the photonic band diagram and keeping the power flow away from dissipation through the transmission line.

Declaration of Competing Interest

The authors declare that they have no known competing financial interests or personal relationships that could have appeared to influence the work reported in this paper.

References

[1] M. Kim, S. Kim, High efficiency dielectric photonic crystal fiber metalens, Sci. Rep. 10 (2020) 20898, https://doi.org/10.1038/s41598-020-77821-5.

[2] X. Mu, S. Wu, L. Cheng, H.Y. Fu, Edge couplers in silicon photonic integrated circuits: a review, Appl. Sci. 10 (2020) 1538, https://doi.org/10.3390/APP10041538.

[3] J. Broeng, D. Mogilevstev, S.E. Barkou, A. Bjarklev, Photonic crystal fibers: a new class of optical waveguides, Opt. Fiber Technol. 5 (1999) 305–330, https://doi.org/10.1006/OFTE.1998.0279.

[4] R. Wang, T. Cao, Reconfigurable slow light in phase change photonic crystal waveguide, J. Appl. Phys. 128 (2020), 163104, https://doi.org/10.1063/5.0020963.

[5] R. Magnusson, Wideband reflectors with zero-contrast gratings, Opt. Lett. 39 (2014) 4337–4340, https://doi.org/10.1364/OL.39.004337.

[6] M.J. Uddin, R. Magnusson, T. Khaleque, Guided-mode resonant polarization-controlled tunable color filters, Opt. Express 22 (2014) 12307–12315, https://doi.org/10.1364/OE.22.012307.

[7] A. Kodigala, T. Lepetit, Q. Gu, B. Bahari, Y. Fainman, B. Kanté, Lasing action from photonic bound states in continuum, Nature 541 (2017) 196–199, https://doi.org/10.1038/nature20799.

[8] T. Cao, C.-W. Wei, M.-J. Chen, B. Guo, Y.-J. Kim, S. Zhang, C.-W. Qiu, A reprogrammable multifunctional chalcogenide guided-wave lens, Nanoscale 10 (2018) 17053–17059, https://doi.org/10.1039/C8NR02100G.

[9] R. Xia, J. Zhu, J. Yi, S. Shao, Z. Li, Guided wave propagation in multilayered periodic piezoelectric plate with a mirror plane, Int. J. Mech. Sci. 204 (2021), 106539, https://doi.org/10.1016/J.IJMECSCI.2021.106539.

[10] T. Cao, L. Fang, Y. Cao, N. Li, Z. Fan, Z. Tao, Dynamically reconfigurable topological edge state in phase change photonic crystals, Sci. Bull. 64 (2019) 814–822, https://doi.org/10.1016/J.SCIB.2019.02.017.

[11] D.J. DiGiovanni, J. Jasapara, R. Bise, R. Windeler, T.H. Her, Group-velocity dispersion measurements in a photonic bandgap fiber, J. Opt. Soc. Am. B 20 (2003) 1611–1615, https://doi.org10.1364/josab.20.001611.

[12] R. Das, Q. Zhang, J. Mukherjee, Synthesis of negative group delay using lossy coupling matrix, 2017. ⟨https://arxiv.org/pdf/1708.02343.pdf⟩, (Accessed 12 September 2018).

[13] J.K. Lucek, K. Smith, All-optical signal regenerator, Opt. Lett. 18 (1993) 1226, https://doi.org/10.1364/OL.18.001226.

[14] H. Kogelnik, R.M. Jopson, L.E. Nelson, Polarization-mode dispersion, in: I. P. Kaminow, T. Li (Eds.), Optical Fiber Telecommunications IV-B, Elsevier, 2002, pp. 725–861.

[15] M. Brodsky, N.J. Frigo, M. Tur, Polarization mode dispersion, in: I.P. Kaminow, T. Li, A.E. Willner (Eds.), Optical Fiber Telecommunications V A, Elsevier, 2008, pp. 605–669.

[16] A.R. Chraplyvy, Optical power limits in multi-channel wavelength-division-multiplexed systems due to stimulated Raman scattering, Electron. Lett. 20 (1984) 58, https://doi.org/10.1049/el:19840040.

[17] S.K. Gupta, A.K. Sarma, Optical parametric amplifications in parity-time symmetric negative-index materials, J. Opt. 47 (2018) 115–120, https://doi.org/10.1007/s12596-017-0429-7.

[18] S. Xiao, V.P. Drachev, A.V. Kildishev, X. Ni, U.K. Chettiar, H.-K. Yuan, V. M. Shalaev, Loss-free and active optical negative-index metamaterials, Nature 466 (2010) 735–738, https://doi.org/10.1038/nature09278.

[19] A. Sommerfeld, L. Brillouin, Wave Propagation and Group Velocity, Academic Press, 1960.

[20] C.D. Broomfield, J.K.A. Everard, Broadband negative group delay networks for compensation of microwave oscillators and filters, Electron. Lett. 36 (2000) 1931–1933, https://doi.org/10.1049/el:20001377.

[21] G.V. Eleftheriades, O. Siddiqui, A.K. Iyer, Transmission line models for negative refractive index media and associated implementations without excess resonators, IEEE Microw. Wirel. Compon. Lett. 13 (2003) 51–53, https://doi.org/10.1109/LMWC.2003.808719.

[22] J. Valentine, S. Zhang, T. Zentgraf, E. Ulin-Avila, D.A. Genov, G. Bartel, X. Zhang, Three-dimensional optical metamaterial with a negative refractive index, Nature 455 (2008) 376–379, https://doi.org/10.1038/nature07247.

[23] V.M. Shalaev, Optical negative-index metamaterials, Nat. Photonics 1 (2007) 41–48, https://doi.org/10.1038/nphoton.2006.49.

[24] S. Moradi, A. Govdeli, S. Kocaman, Zero average index design via perturbation of hexagonal photonic crystal lattice, Opt. Mater. 73 (2017) 577–584, https://doi.org/10.1016/j.optmat.2017.09.008.

[25] J.J. Sakurai, S.F. Tuan, E.D. Commins, Modern quantum mechanics, revised edition, Am. J. Phys. 63 (1995) 93–95, https://doi.org/10.1119/1.17781.

[26] J. Joannopoulos, S. Johnson, J. Winn, R. Meade, Photonic Crystals: Molding the Flow of Light, 2011.

[27] J. Thijssen, Characterization of Photonic Colloidal Crystals in Real and Reciprocal Space (Doctoral thesis), Utrecht University, 2007. ⟨https://dspace.library.uu.nl/handle/1874/21249⟩.

[28] J.D. Joannopoulos, S.G. Johnson, Block-iterative frequency-domain methods for Maxwell's equations in a planewave basis, Opt. Express 8 (2001) 173–190, https://doi.org/10.1364/OE.8.000173.

[29] H. Mao, J. Wang, K. Yu, Z. Zhu, TM and TE propagating modes of photonic crystal waveguide based on honeycomb lattices, Appl. Opt. 49 (2010) 6597–6601, https://doi.org/10.1364/AO.49.006597.

[30] R. Magnusson, S.-G. Lee, Essential differences between TE and TM band gaps in periodic films at the first Bragg condition, Opt. Lett. 44 (2019) 4658–4661, https://doi.org/10.1364/OL.44.004658.

[31] AbInitio, Meep tutorial, 2017. ⟨http://ab-initio.mit.edu/wiki/index.php/Meep_tutorial⟩, (Accessed 8 May 2018).